Appl. Phys. A (2017) 123:488
DOI 10.1007/s00339-017-1115-y

Applied Physics A
Materials Science & Processing

Effect of composition and temperature on the magnetic properties of $BaBi_xLa_xFe_{(12-2x)}O_{19}$ ($0.0 \leq x \leq 0.2$) hexaferrites

Ramazan Topkaya[1]

Received: 13 March 2017 / Accepted: 27 June 2017 / Published online: 29 June 2017

Abstract Bi–La-substituted M-type barium hexaferrites, $BaBi_xLa_xFe_{(12-2x)}O_{19}$ ($0.0 \leq x \leq 0.2$), were prepared by the standard solid-state reaction method. The effect of temperature and concentration on the structural and magnetic properties of $BaBi_xLa_xFe_{(12-2x)}O_{19}$ hexaferrite powders has been comprehensively investigated. XRD analysis confirms the formation of M-type hexagonal crystal structure with $P6_3/mmc$ space group. The average crystallite size of the powders was determined using Scherrer's formula (in the range of 66–77 nm.). Lattice parameters were found to increase with the increase in Bi–La substitution. Magnetic properties were enhanced by substitution. Magnetic hysteresis loops were analysed using a 'Law of Approach to Saturation' method. It was obtained the saturation magnetization value close to the bulk value. Bi–La substitution gives rise to increase of saturation magnetization, coercive field, and effective magnetic anisotropy constant for both 10 and 300 K. It is observed from FMR measurements that resonance field increases with the concentration. The broad FMR linewidth of almost 2.5 kOe indicates the existence of the particles with randomly distributed anisotropy axis. The enhanced magnetic properties make these powders a good candidate for potential applications in permanent magnets at low cost and microwave absorption devices.

✉ Ramazan Topkaya
ramazan.topkaya@igdir.edu.tr

[1] Department of Electrical Electronics Engineering, Faculty of Engineering, Iğdır University, 76000 Iğdır, Turkey

1 Introduction

M-type hexagonal ferrites with its stoichiometric chemical formula $BaFe_{12}O_{19}$ (generally denoted as BaM) have been paid more attention in the last few decades because of their potential applications in permanent magnet at low cost, high-density magnetic recording, next-generation microwave devices, magnetic fluids, and catalysts [1–7]. They have magnetic, chemical, and dielectric properties such as high coercivity, high saturation magnetization, high Curie temperature, corrosion resistance, and good chemical stability [2, 7]. Barium hexaferrites have magnetically hard property due to their large magnetic anisotropy with c-axis easy magnetization. They are used as a magnetic material for the permanent magnet application at low cost because of this property [8]. In addition, they can be used as a microwave absorber in microwave applications for a broad frequency range due to their large permeability [1]. The magnetic properties of the hexaferrites should be tailored with different techniques and methods to make them suitable for the above-mentioned different applications [9–11].

It is known that M-type barium hexagonal ferrites have five different crystallographic sites or sublattices (bipyramidal 2b, tetragonal $4f_1$, and octahedral 2a, 12k, and $4f_2$). Fe^{3+} ions located on these different sites determine the magnetic properties of the hexaferrites [12]. The substitution of Fe^{3+} ions by different ions having larger ionic radii compared with the Fe ion radius can be an effective way to tailor the magnetic properties (like magnetization, coercive field, and magnetic anisotropy constant, etc.) for the above-mentioned applications. Many different cations have been used for this purpose, such as Y^{3+}, Ti^{2+}, Ni^{2+}, Al^{3+}, Ga^{3+}, and Cr^{3+} [13–17].

These modifications have been come out to cause the significant changes in the magnetic and electrical

properties [18–24]. For example, with the diamagnetic substitutions (Al and In), the invar effect has been observed in barium hexaferrite solid solutions in low-temperature range [22, 24]. Dual ferroic properties (coexistence of magnetization and polarization) have been revealed at room temperature for Al-substituted barium hexaferrite ceramics ($BaFe_{12-x}Al_xO_{19}$) in recent years [25, 26]. In addition, the substitution of La ions gives rise to increase coercive field and saturation magnetization [27–29]. This increment is related to the increase of magnetocrystalline anisotropy constant. Many of the previous investigations about Bi–La-doped hexaferrites have been done at room temperature [20, 28, 29].

In this study, the concentration and temperature dependence of the magnetic properties were investigated in a wide range of temperature (10–300 K) and magnetic fields (±50 kOe) in an attempt to find out in detail the magnetic behaviour of these powders. The enhancement of the magnetic properties of the barium hexaferrites substituted with Bi–La ions was presented. It was discussed in detail the reasons of improving of the magnetic properties (coercive field, magnetization, effective magnetic anisotropy, and resonance field) as a function of concentration and temperature.

2 Experimental details

Bi–La-substituted barium hexaferrite powders with general formula $BaBi_xLa_xFe_{(12-2x)}O_{19}$ ($0.0 \leq x \leq 0.2$) were prepared by the standard solid-state reaction method. The chemicals Fe_2O_3, $Ba(CH_3COO)_2$, Bi_2O_3, La_2O_3, and B_2O_3 were used for the synthesis. They were mixed for 20 min and precalcinated at 500 °C for 2 h and finally calcinated at 1000 °C for 2 h. The crystal structure was analysed using Rigaku SmartLab X-ray diffractometer (XRD) with Cu-K_α radiation. The magnetization measurements were carried out by vibrating sample magnetometer (VSM, Quantum Design, PPMS 9 T) as a function of magnetic field and temperature in the magnetic field of ±50 kOe and in the temperature range of 10–300 K. Ferromagnetic resonance (FMR) spectra were recorded using Bruker EMX X-band spectrometer (9.8 GHz). The static magnetic field was varied in the range of 6–22 kOe. The field derivative of microwave power absorption (dP/dH) was recorded as a function of the static magnetic field (H) at room temperature (300 K).

3 Results and discussion

3.1 XRD analysis

Figure 1 shows XRD powder patterns for $BaBi_xLa_xFe_{(12-2x)}O_{19}$ ($0.0 \leq x \leq 0.2$) hexaferrite powders. The patterns are in good agreement with JCPDS data (card no. 039-1433), confirming the formation of the hexagonal crystal structure (space group $P6_3/mmc$, 194). Some smaller peaks corresponding to α-Fe_2O_3 were observed in the powders with $x = 0.0$ and 0.1 due to an incomplete crystallization. The average crystallite size (D) was calculated from (114) diffraction peak using Scherrer's formula and listed in Table 1. The lattice parameters ($a = b$, c) were calculated by the following equation:

$$\frac{1}{d^2} = \frac{4}{3}\left(\frac{h^2 + hk + k^2}{a^2}\right) + \frac{l^2}{c^2} \quad (1)$$

where d is spacing value and h, k, and l values are the Miller indices belonging to XRD diffraction peaks. Figure 2 shows the variation of the calculated lattice parameters with Bi–La concentration (also listed in Table 1). As can be easily seen, the lattice parameters continuously increase with Bi–La concentration. Lattice constant depends on the ionic radii, electron affinity, bond length, and oxidation state [30]. The interaction among the neighbour atoms influences the bond length between the atoms and, therefore, the lattice constants [30]. Moreover, the substitution of metals with larger ionic radii for Fe with smaller ionic radii brings about the increasing of the lattice parameters [31]. Because the ionic radii of Bi^{3+} and La^{3+} (0.96 and 1.03 Å, respectively) are larger than that of Fe^{3+} (0.64 Å) [32, 33], the lattice parameters and, thus, the cell volume (V) increase with the concentration in this study. The similar behaviour has been observed for Zr–Cu-substituted strontium hexaferrite nanoparticles [31] and $BaCu_xMg_xZr_{2x}Fe_{12-4x}O_{19}$ hexaferrite nanoparticles [34]. According to Wagner, the structure can be assumed as the M-type magnetoplumbite structure if the c/a ratio is obtained to be lower than 3.98 [35]. As can be seen from Table 1, the c/a ratio ranges from 3.940 to 3.937, which is lower than 3.98. This confirms the formation of M-type

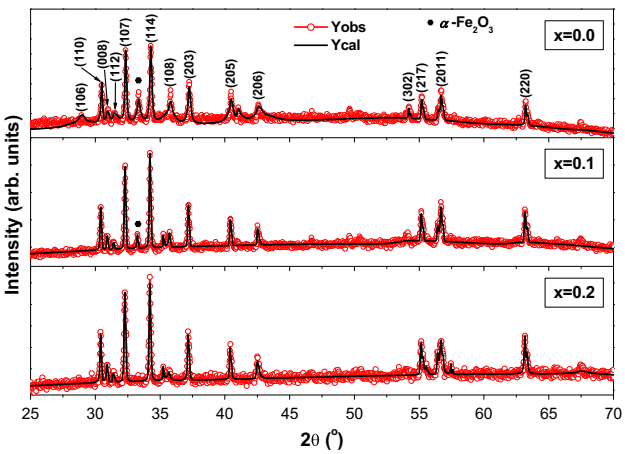

Fig. 1 X-ray diffraction patterns of $BaBi_xLa_xFe_{(12-2x)}O_{19}$ ($0.0 \leq x \leq 0.2$) hexaferrite powders

Table 1 Bi–La content, lattice parameters (a, b, c), c/a ratio, volume, and crystallite size of $BaBi_xLa_xFe_{(12-2x)}O_{19}$ ($0.0 \leq x \leq 0.2$) hexaferrite powders

Bi–La content (x)	Lattice parameters		c/a	V (Å)^3	Crystallite size (nm)
	$a = b$ (Å)	c (Å)			
0.0	5.858	23.081	3.940	685.92	66
0.1	5.863	23.110	3.942	687.95	77
0.2	5.877	23.139	3.937	692.11	75

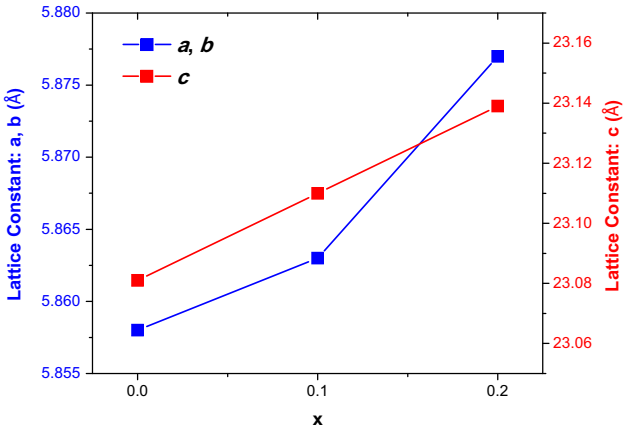

Fig. 2 Variation of lattice constants a, b, and c with composition (x) for $BaBi_xLa_xFe_{(12-2x)}O_{19}$ ($0.0 \leq x \leq 0.2$) hexaferrite powders

hexagonal magnetoplumbite structure for $BaBi_xLa_xFe_{(12-2x)}O_{19}$ ($0.0 \leq x \leq 0.2$) hexaferrite powders.

3.2 VSM analysis

Figure 3 shows the magnetization curves (M–H curves) of $BaBi_xLa_xFe_{(12-2x)}O_{19}$ ($0.0 \leq x \leq 0.2$) hexaferrite powders for 300 (a) and 10 K (b). M–H curves of all the samples were obtained by changing the external magnetic field up to ±50 kOe to saturate the samples. The observed hysteretic behaviour of the samples used in the present study indicates that $BaBi_xLa_xFe_{(12-2x)}O_{19}$ ($0.0 \leq x \leq 0.2$) hexaferrite powders have ferromagnetic behaviour in the temperature range of 10–300 K.

It is known that at a sufficiently high magnetic field, the variation of the magnetization follows "Law of Approach to Saturation" [36, 37]. Therefore, magnetization (M) and applied high magnetic field (H) depend on each other as follows:

$$M = M_s\left[1 - \frac{A}{H} - \frac{B}{H^2}\right] + \chi H \tag{2}$$

where M_s is saturation magnetization. The term A/H is related to the magnetic anisotropy resulting from the inhomogeneity of the material. The term B/H^2 is related to the magnetocrystalline anisotropy of the material. χ is high-field susceptibility. The terms A/H and χ vanish at high magnetic fields. For the material with hexagonal crystal structure, K_{eff} and H_a can be written as

$$K_{eff} = M_s\sqrt{\frac{15B}{4}} \tag{3}$$

$$H_a = 2\frac{K_{eff}}{M_s}, \tag{4}$$

where K_{eff} and H_a are effective magnetic anisotropy constant and magnetic anisotropy field, respectively. After the fitting of M-$1/H^2$ plots with Law of Approach to Saturation method, the intersection of the straight line with magnetization axis gives the saturation magnetization. The slope of the straight line is used to determine the effective magnetic anisotropy constant and magnetic anisotropy field.

Figure 4 shows the magnetization (M) vs $1/H^2$ plots of $BaBi_xLa_xFe_{(12-2x)}O_{19}$ ($0.0 \leq x \leq 0.2$) hexaferrite powders for 300 (a) and 10 K (b). It can be easily seen the linear relation between M and $1/H^2$ for each sample and temperature. According to Eq. (2), the linear fit of the M vs $1/H^2$ plots gives the saturation magnetization (Ms), slope (M_SB), and also the magnetic parameter B values. As a function of Bi^{3+} and La^{3+} concentrations (x), the variation of saturation magnetization (M_s) of $BaBi_xLa_xFe_{(12-2x)}O_{19}$ ($0.0 \leq x \leq 0.2$) hexaferrite powders for both 300 and 10 K is shown in Fig. 5. It can be easily seen that the saturation magnetization continuously increases with increasing the Bi^{3+} and La^{3+} concentrations from $x = 0.0$–0.2 and reaches its maximum value at $x = 0.2$. This behaviour is the same for both 300 and 10 K as can be easily seen in Fig. 5. The highest M_s values were recorded for the concentration $x = 0.2$ and are 64.40 and 91.57 emu/g for 300 and 10 K, respectively. These values are close to bulk values of barium hexaferrite ($BaFe_{12}O_{19}$) [38] for both 300 and 10 K. The saturation magnetization values close to bulk values make the powders used in this study a promising candidate for different industrial applications. Moreover, the saturation magnetization values obtained in the present study are higher than that of La-doped barium hexaferrite powders synthesized in ammonium nitrate melt [9], Ba hexaferrites doped with bismuth oxide [32], and modified Z-type hexaferrite with Bi_2O_3 additive [39].

The crystal structure of barium hexaferrites ($BaFe_{12}O_{19}$) with magnetoplumbite structure consists of five crystallographic sites: three octahedral sites ($2a$, $12k$, and $4f_2$), one

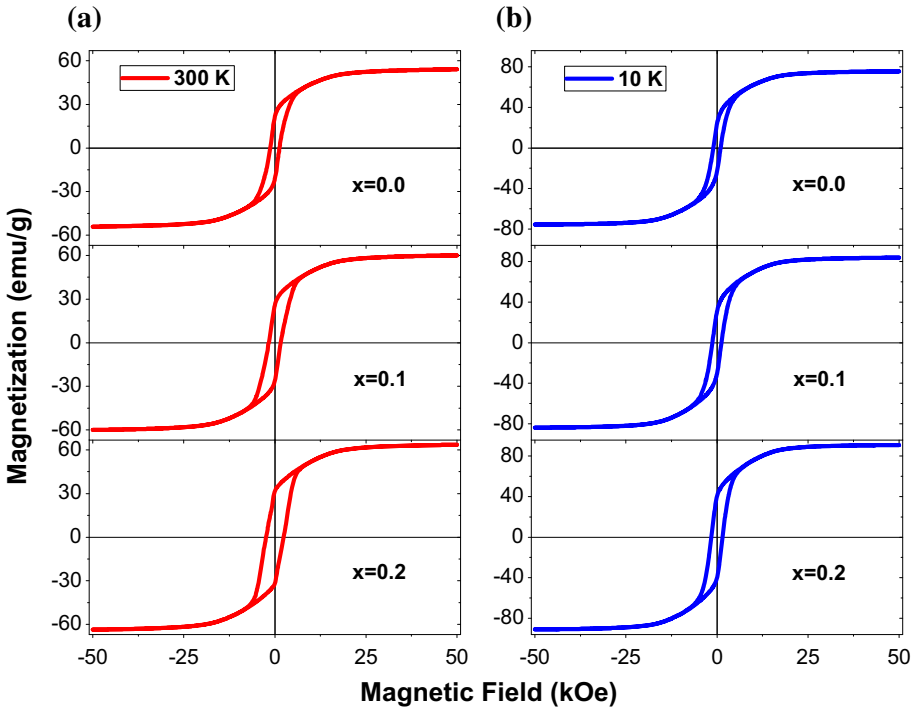

Fig. 3 Concentration-dependent magnetic hysteresis loops of $BaBi_xLa_xFe_{(12-2x)}O_{19}$ ($0.0 \leq x \leq 0.2$) hexaferrite powders for 300 (**a**) and 10 K (**b**)

tetrahedral site ($4f_1$), and one trigonal-bi-pyramidal site ($2b$) [2]. Their magnetic behaviour results from the magnetic moment of the Fe^{3+} ions. All the Fe^{3+} ions in the hexaferrite crystal structure are distributed on these sites. The Fe^{3+} ions in the three parallel sites ($2a$, $2b$, and $12k$) are have upward spin direction, whereas these in the two anti-parallel sites ($4f_1$ and $4f_2$) have downward spin direction. Thus, the total magnetic moment or magnetization is determined by the algebraic sum of the magnetic moments of the Fe^{3+} ions in the sites:

$$m = (m_{2a} + m_{2b} + m_{12k})_{\uparrow} + (m_{4f_1} + m_{4f_2})_{\downarrow} \quad (5)$$

where m indicates the magnetic moment or magnetization of Fe^{3+} ions in each site and the arrows (↑ and ↓) show upward and downward spin directions.

The variation of the saturation magnetization with the nonmagnetic Bi^{3+} and La^{3+} contents is unveiled with the preferential crystallographic site occupancy of the substituted Bi^{3+} and La^{3+} ions at different sublattice sites [12, 40, 41]. If the nonmagnetic La^{3+} and Bi^{3+} ions enter $4f_1$ and $4f_2$ sites (spin-down sites) or substitute by the Fe^{3+} ions in these sites, the net magnetic moment (or magnetization) increases. Therefore, the saturation magnetization of $BaBi_xLa_xFe_{(12-2x)}O_{19}$ ($0.0 \leq x \leq 0.3$) hexaferrites increases with increasing the Bi–La substitution contents up to $x = 0.2$. The similar behaviour of the saturation magnetization was reported for La–Co substituted M-type barium ferrites [42] and Co–Ru substituted Ba–Sr hexagonal ferrite powders [43]. In general, the net magnetic moment (or magnetization) originates from the super exchange interactions between transition-metal ions mediated by the oxygen atoms in oxides (Fe^{3+}–O–Fe^{3+}). The strengthening of the superexchange interaction gives rise to increase the net magnetic moment of the hexaferrite [29].

Figure 6 represents the variation of the effective magnetic anisotropy (K_{eff}) and anisotropy field (H_a) values with respect to Bi^{3+} and La^{3+} concentrations (x) for both 300 and 10 K. As can be easily seen from Fig. 6, K_{eff} increases, whereas H_a decreases with rise in Bi^{3+} and La^{3+} concentrations (x). It is known that the large magnetocrystalline anisotropy of the barium hexaferrite results from the strong exchange interaction among Fe^{3+} ions on the 2b and $4f_2$ sites [44]. The increment in K_{eff} may be attributed to the increasing the crystallinity of powders [45]. The competition between K_{eff} and M_s determines the variation of H_a with respect to the substitution as dictated by Eq. (4). The saturation magnetization (M_s) (Fig. 5) increases more rapidly than the effective magnetic anisotropy constant (K_{eff}) (Fig. 6) with the increase of the Bi^{3+} and La^{3+} concentrations (x), which cause the anisotropy field to decrease for both 300 and 10 K.

Figure 7 shows the variation of the saturation magnetization (M_s) of $BaBi_xLa_xFe_{(12-2x)}O_{19}$ ($0.0 \leq x \leq 0.2$) hexaferrite powders with temperature. It can be seen from the figure that M_s continuously decreases as temperature increases from 10 to 300 K for each concentration. This is due to the weakening of the Fe^{3+}–O–Fe^{3+} superexchange interactions between Fe^{3+} ions with the increasing of the temperature from 10 to 300 K.

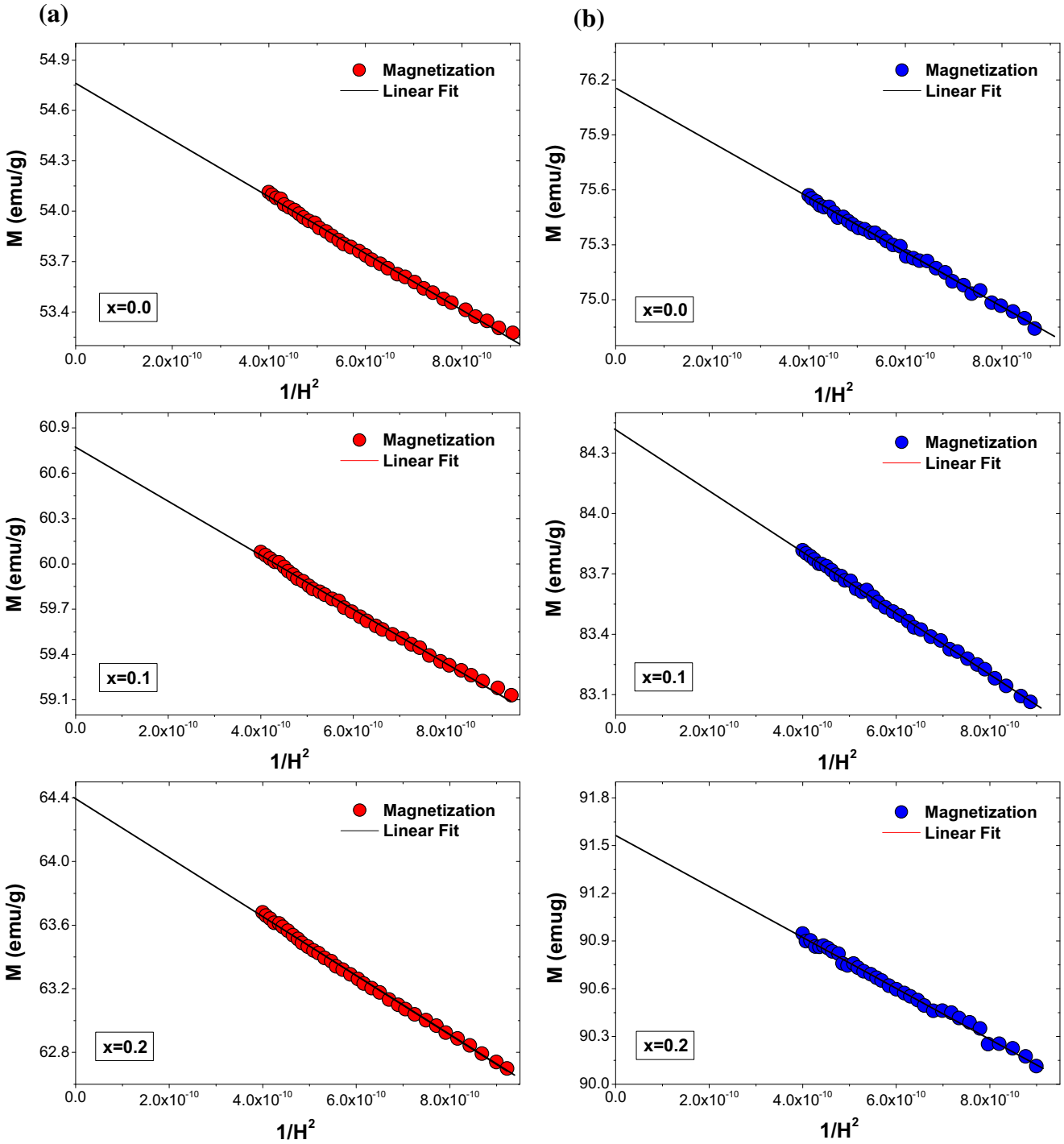

Fig. 4 Magnetization (M) vs. $1/H^2$ plots for $BaBi_xLa_xFe_{(12-2x)}O_{19}$ ($0.0 \leq x \leq 0.2$) hexaferrite powders recorded at **a** 300 and **b** 10 K

Bi–La concentration dependence of coercive field (H_c) of $BaBi_xLa_xFe_{(12-2x)}O_{19}$ ($0.0 \leq x \leq 0.2$) hexaferrite powders for 300 and 10 K is shown in Fig. 8. As can be seen, H_c increases by approximate two times as the Bi–La concentration increases from $x = 0.0$–0.2. It should be noted that the nonmagnetic Bi^{3+} and La^{3+} ions are very effective in the increase in the strength of the coercive field. It is known to be observed a high coercive field for barium hexaferrite because of having a strong uniaxial magnetic anisotropy [46]. The observed increase in H_c with the increase in the Bi–La concentration (x) is due to the enhancement of the effective magnetic anisotropy (Fig. 6a). The variation trend of the coercive and anisotropy field with Bi^{3+} and La^{3+} concentrations is not similar

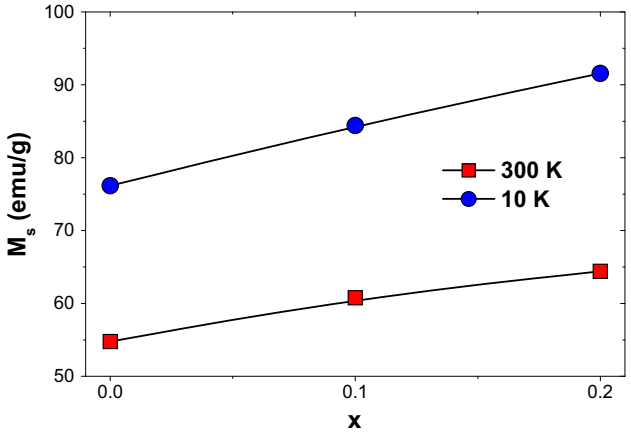

Fig. 5 Variation of saturation magnetization (M_s) of $BaBi_xLa_xFe_{(12-2x)}O_{19}$ ($0.0 \leq x \leq 0.2$) hexaferrite powders with Bi^{3+} and La^{3+} concentration (x) at 300 and 10 K

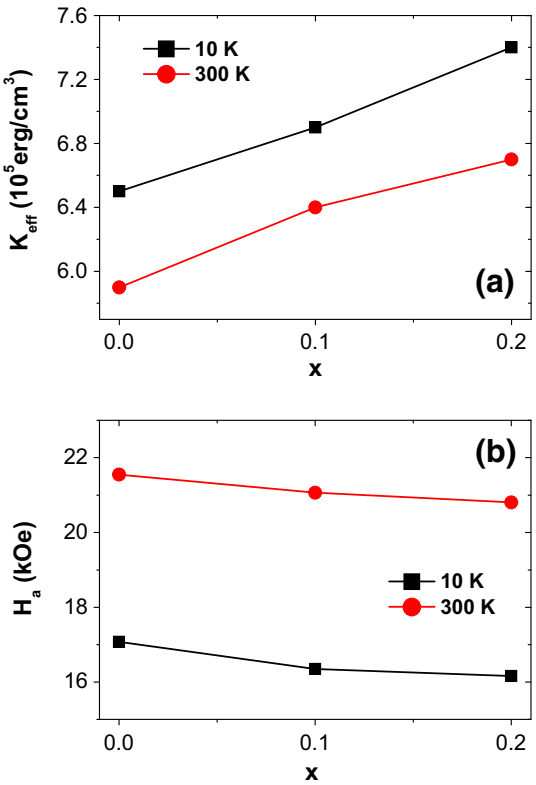

Fig. 6 Concentration (x) dependence of effective magnetic anisotropy constant (K_{eff}) (**a**) and anisotropy field (H_a) (**b**) calculated using Law of Approach to Saturation method for $BaBi_xLa_xFe_{(12-2x)}O_{19}$ ($0.0 \leq x \leq 0.2$) hexaferrite powders

to each other. This means that the magnetocrystalline anisotropy of the samples is not the dominant factor affecting the magnetization reversal processes of the particles [18, 43].

The temperature dependence of the coercive field (H_c) values of $BaBi_xLa_xFe_{(12-2x)}O_{19}$ ($0.0 \leq x \leq 0.2$) hexaferrite

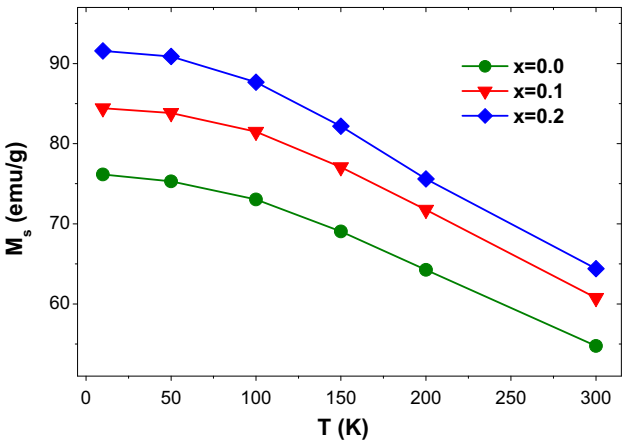

Fig. 7 Dependence of saturation magnetization (M_s) of $BaBi_xLa_xFe_{(12-2x)}O_{19}$ ($0.0 \leq x \leq 0.2$) hexaferrite powders on temperature

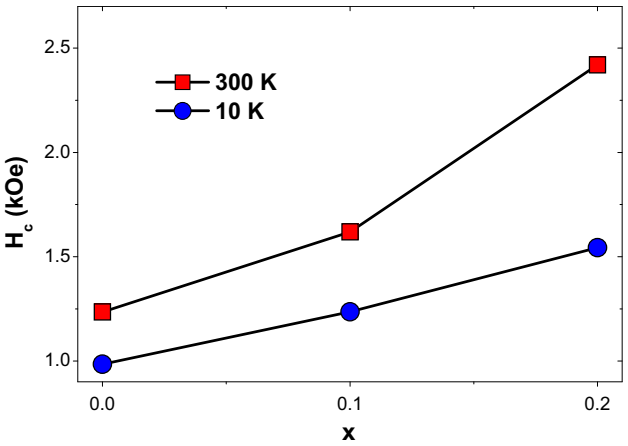

Fig. 8 Dependence of coercive field (H_c) of $BaBi_xLa_xFe_{(12-2x)}O_{19}$ ($0.0 \leq x \leq 0.2$) hexaferrites on Bi–La concentration (x) for 300 and 10 K

powders is shown in Fig. 9. It is easily seen that the coercive field is strongly influenced by temperature. It is known that the coercive field is the required magnetic field for the magnetization reversal processes [36]. According to the Stoner–Wohlfarth theory, coercive field increases with the increasing of magnetic anisotropy constant, whereas decreases with the increasing of saturation magnetization [47]. The variation of the coercive field depends on the competition between magnetic anisotropy constant and saturation magnetization. In this study, the decreasing of H_c with decreasing temperature is attributed to the saturation magnetization increasing more rapidly than the effective magnetic anisotropy constant (K_{eff}) calculated from the linear fitting of M vs $1/H^2$ curves.

3.3 FMR analysis

The room temperature FMR spectra of $BaBi_xLa_xFe_{(12-2x)}O_{19}$ ($0.0 \leq x \leq 0.2$) hexaferrite powders are presented in

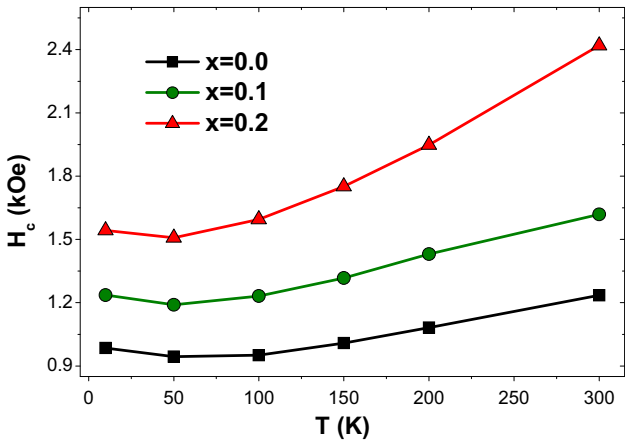

Fig. 9 Dependence of coercive field (H_c) of $BaBi_xLa_xFe_{(12-2x)}O_{19}$ ($0.0 \leq x \leq 0.2$) hexaferrite powders on temperature

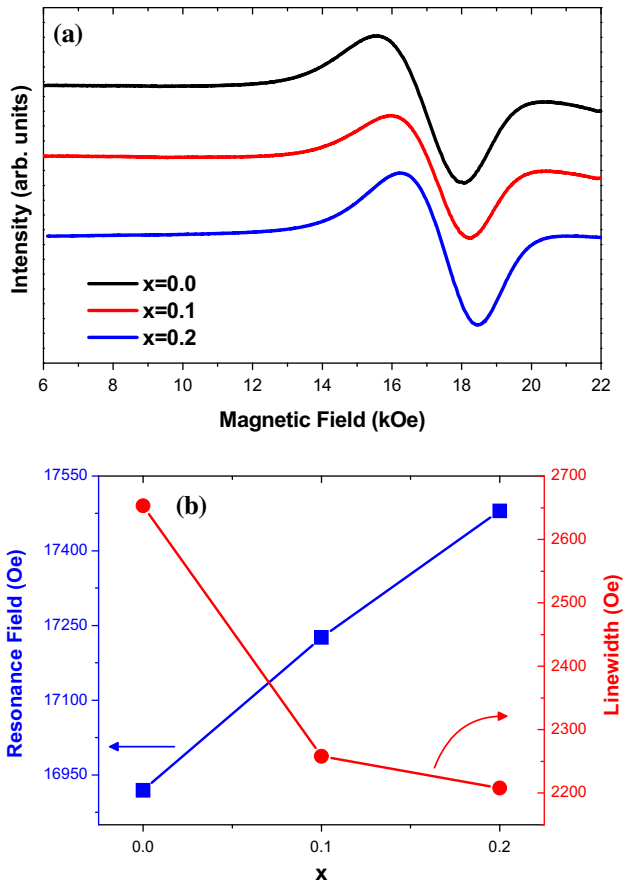

Fig. 10 **a** FMR spectra of $BaBi_xLa_xFe_{(12-2x)}O_{19}$ ($0.0 \leq x \leq 0.2$) hexaferrite powders, **b** variation of resonance field and linewidth of FMR spectra with respect to Bi–La concentration (x)

Fig. 10a. As can be easily seen from Fig. 10a, b, the resonance fields of the FMR spectra are high (almost 17 kOe) for each powder and increases with Bi–La concentration (x). These high resonance field values are due to the magnetically hard property of barium hexaferrite. In addition, all the FMR spectra are characterized by a single, broad, and slightly asymmetric resonance line. The broad curves indicate that the powders used in this study have ferromagnetic behaviour. In addition, the broad lines prove the existence of dipolar–dipolar interactions among particles and randomly oriented magnetic anisotropy axes [41, 48, 49]. The asymmetric behaviour is related to the non-uniform modes as well as the main FMR mode [37, 41]. As the Bi–La concentration (x) increase, the peak-to-peak FMR linewidth decreases from 2653 to 2208 Oe. As is known, the FMR linewidth (ΔH_{pp}) of polycrystalline ferrite is given by [50–52]

$$\Delta H_{pp} = \Delta H_i + \Delta H_a + \Delta H_p \quad (6)$$

where ΔH_i is the linewidth of single crystal or intrinsic linewidth, ΔH_a is the crystalline anisotropy induced linewidth broadening contribution, and ΔH_p is the porosity-induced linewidth broadening contribution. ΔH_i is small (on the order of few Oe) when comparing with other linewidth contributions [50]. Therefore, ΔH_i is usually neglected. In this case, the main contribution to ΔH_{pp} comes from ΔH_a and ΔH_p. It has been shown in the works of R. Guo and X. Jiang et al. [50, 51] that ΔH_a is almost unchanged with increasing the iron deficiency or concentration of Bi_2O_3 in Bi-doped polycrystalline ferrites. According to ferromagnetic relaxation theory, porosity is one of the dominant factors affecting FMR linewidth in bulk polycrystalline ferrites [51]. In Bi-doped polycrystalline ferrites, porosity slowly decreases with increasing Bi^{3+} concentration [50]. In addition, it has been observed that the variation of the porosity-induced linewidth contribution is almost the same that of FMR linewidth with respect to rise in Bi^{3+} concentration [50, 51]. In this way, the decrease in porosity brings about the decline of FMR linewidth. Therefore, with rise in Bi^{3+} concentration (x), the decreasing of ΔH_{pp} can be attributed to the porosity in the powders in this work.

Moreover, the broad FMR linewidth indicates that the powders absorb the microwave in the broad absorption range. This makes the powders used in this study a good candidate for radar-absorbing materials (RAMs) used in microwave absorption applications in broad frequency range.

4 Conclusion

Bi–La-substituted M-type barium hexaferrites, $BaBi_xLa_xFe_{(12-2x)}O_{19}$ ($0.0 \leq x \leq 0.2$), were prepared by the standard solid-state reaction method. The structural and magnetic properties of the powders were investigated in detail in the temperature from 10 to 300 K under magnetic field of ± 50 kOe. The structural properties of the powders were

analysed by X-ray diffraction (XRD) technique. The magnetic properties were determined using vibrating sample magnetometer (VSM) and ferromagnetic resonance (FMR) techniques. All the powders show the magnetoplumbite-type hexagonal crystal structure characteristic. The average crystallite size of the powders was found to be in the range of 66–77 nm. It has been observed that Bi–La doping contributes to the improvement of magnetic properties. Law of Approach to Saturation method is used to determine the saturation magnetization, effective anisotropy constant, and anisotropy field. The saturation magnetization and effective magnetic anisotropy constant increase with the increasing of Bi–La concentration (x). The coercivity value increases with increasing Bi–La concentration due to an enhancement of effective magnetic anisotropy. FMR measurements prove the ferromagnetic behaviour of the powders. The resonance field increases, whereas linewidth decreases with increasing the Bi–La concentration. The broad FMR linewidth originates from the random orientation of magnetic anisotropy axis. VSM and FMR measurements reveal that these powders are a good candidate for the potential applications in permanent magnet and microwave absorption devices.

References

1. S.S.S. Afghahi, M. Jafarian, Y. Atassi, J. Mag. Mag. Mater. **419**, 62 (2016)
2. H. Kojima, Handb. Ferromagn. Mater. **3**, 305 (1982)
3. G. Sahin, Appl. Phys. A **122**, 997 (2016)
4. G. Sahin, Results Phys. **6**, 107 (2016)
5. A. Guler, C. Boyraz, J. Supercond. Nov. Magn. (2016). doi:10.1007/s10948-016-3854-y
6. C. Boyraz, A. Guler, M. Ozdemir, Y. Oner, J. Supercond. Nov. Magn. **30**, 1145 (2017)
7. H. Pfeiffer, R.W. Chantrell, P. Görnert, W. Schüppel, E. Sinn, M. Rösler, J. Mag. Mag. Mater. **125**, 373 (1993)
8. R. Tang, C. Jiang, H. Zhou, H. Yang, J. Alloy. Compd. **658**, 132 (2016)
9. I. Kucuk, H. Sözeri, H. Özkan, J. Supercond. Nov. Magn. **24**, 1333 (2011)
10. I. Ali, M.U. Islam, M.S. Awan, M. Ahmad, J. Alloy. Compd. **547**, 118 (2013)
11. S. Dursun, R. Topkaya, N. Akdoğan, S. Alkoy, Ceram. Int. **38**, 3801 (2012)
12. R. Topkaya, I. Auwal, A. Baykal, Ceram. Int. **42**, 16296 (2016)
13. I. Auwal, H. Güngüneş, S. Güner, S.E. Shirsath, M. Sertkol, A. Baykal, Mater. Res. Bull. **80**, 263 (2016)
14. A. Awadallah, S.H. Mahmood, Y. Maswadeh, I. Bsoul, M. Awawdeh, Q.I. Mohaidat, H. Juwhari, Mater. Res. Bull. **74**, 192 (2016)
15. M. Awawdeh, I. Bsoul, S. Mahmood, J. Alloy. Compd. **585**, 465 (2014)
16. I. Bsoul, S.H. Mahmood, A.-F. Lehlooh, J. Alloy. Compd. **498**, 157 (2010)
17. X. Tang, Y. Yang, K. Hu, J. Alloy. Compd. **477**, 488 (2009)
18. H. Fang, Z. Yang, C. Ong, Y. Li, C. Wang, J. Mag. Mag. Mater. **187**, 129 (1998)
19. T. Kaur, S. Kumar, B.H. Bhat, B. Want, A. Srivastava, Appl. Phys. A **119**, 1531 (2015)
20. X. Shen, M. Liu, F. Song, Y. Zhu, Appl. Phys. A **104**, 109 (2011)
21. A. Trukhanov, S. Trukhanov, L. Panina, V. Kostishyn, I. Kazakevich, A.V. Trukhanov, E. Trukhanova, V. Natarov, V. Turchenko, M. Salem, J. Mag. Mag. Mater. **426**, 487 (2017)
22. A. Trukhanov, V. Turchenko, I. Bobrikov, S. Trukhanov, I. Kazakevich, A. Balagurov, J. Mag. Mag. Mater. **393**, 253 (2015)
23. S. Trukhanov, A. Trukhanov, V. Kostishyn, L. Panina, V. Turchenko, I. Kazakevich, A.V. Trukhanov, E. Trukhanova, V. Natarov, A. Balagurov, J. Mag. Mag. Mater. **426**, 554 (2017)
24. S. Trukhanov, A. Trukhanov, V. Turchenko, V. Kostishin, L. Panina, I. Kazakevich, A. Balagurov, J. Mag. Mag. Mater. **417**, 130 (2016)
25. S. Trukhanov, A. Trukhanov, V. Kostishin, L. Panina, I. Kazakevich, V. Turchenko, V. Kochervinskii, JETP Lett. **103**, 100 (2016)
26. A.V. Trukhanov, S.V. Trukhanov, L.V. Panina, V.G. Kostishyn, D.N. Chitanov, S.K. Il'ya, A.V. Trukhanov, V.A. Turchenko, M.M. Salem, Ceram. Int. **43**, 5635 (2017)
27. Y. Yang, F. Wang, J. Shao, D. Huang, Z. Gao, Q. Cao, M. Wan, J. Mater. Res. **30**, 1844 (2015)
28. W. Li, X. Qiao, M. Li, T. Liu, H.X. Peng, Mater. Res. Bull. **48**, 4449 (2013)
29. S. Ounnunkad, Solid State Commun. **138**, 472 (2006)
30. T. Kaur, S. Kumar, B.H. Bhat, A.K. Srivastava, J. Mater. Res. **30**, 2753 (2015)
31. M.J. Iqbal, M.N. Ashiq, Chem. Eng. J. **136**, 383 (2008)
32. M. Pal, P. Brahma, D. Chakravorty, D.C. Agrawal, J. Mag. Mag. Mater. **147**, 208 (1995)
33. Y.M. Al Angari, J. Mag. Mag. Mater. **323**, 1835 (2011)
34. H. Nikmanesh, M. Moradi, G.H. Bordbar, R. Shams Alam, J. Alloy. Compd. **708**, 99 (2017)
35. T. Wagner, J. Solid State Chem. **136**, 120 (1998)
36. S. Chikazumi, *Physics of Ferromagnetism* (Oxford University Press, Oxford, 1997)
37. R. Topkaya, Ö. Akman, S. Kazan, B. Aktaş, Z. Durmus, A. Baykal, J. Nanopart. Res. **14**, 1 (2012)
38. B.D. Cullity, C. D. Graham, *Introduction to Magnetic Materials*, 2nd edn. (Wiley, New York, 2009)
39. H. Zhang, J. Zhou, Y. Wang, L. Li, Z. Yue, Z. Gui, IEEE Trans. Magn. **38**, 1797 (2002)
40. A. Ghasemi, J. Supercond. Nov. Magn. **29**, 169 (2016)
41. R. Topkaya, A. Baykal, A. Demir, J. Nanopart. Res. **15**, 1 (2013)
42. L. Jie, H. Zhang, L. Qiang, L. Yuanxun, Y. Guoliang, J. Rare Earth. **31**, 983 (2013)
43. C. Singh, S.B. Narang, I. Hudiara, Y. Bai, F. Tabatabaei, Mater. Res. Bull. **43**, 176 (2008)
44. M. Xiao-Mei, L. Jie, Z. Sheng-Zhi, S. Hui-Gang, Chin. Phys. B **25**, 126102 (2016)
45. M. Ganjali, M. Ganjali, A. Eskandari, M. Aminzare, J. Adv. Mater. Pro. **1**, 41 (2013)
46. M.H. Shams, A.S. Rozatian, M.H. Yousefi, J. Valíček, V. Šepelák, J. Mag. Mag. Mater. **399**, 10 (2016)
47. E.C. Stoner, E.P. Wohlfarth, IEEE Trans. Magn. **27**, 3475 (1991)
48. P. Goel, M. Arora, A.M. Biradar, J. Appl. Phys. **115**, 124905 (2014)
49. A. Sukhov, K.D. Usadel, U. Nowak, J. Mag. Mag. Mater. **320**, 31 (2008)
50. R. Guo, Z. Yu, Y. Yang, X. Jiang, K. Sun, C. Wu, Z. Xu, Z. Lan, J. Alloy. Compd. **589**, 1 (2014)
51. X. Jiang, W. Wang, Z. Yu, K. Sun, Z. Lan, X. Zhang, V.G. Harris, AIP Adv. **7**, 1 (2017)
52. E. Schlömann, J. Phys. Radium **20**, 327 (1959)